Electronic Supplementary Material (ESI) for Physical Chemistry Chemical Physics.

Supporting information: De novo prediction of cross-effect efficiency for magic angle spinning dynamic nuclear polarization

Frédéric Mentink-Vigier,[a-b] Anne-Laure Barra,[c] Johan van Tol,[b] Sabine Hediger,[a] Daniel Lee,[a] Gaël De Paëpe[a*]

a Univ. Grenoble Alpes, CEA, CNRS, INAC-MEM, F-38000 Grenoble, France.
b National High Magnetic Field Laboratory, Tallahassee, FL, 32301, USA
c Laboratoire National des Champs Magnétiques Intenses – CNRS, Univ. Grenoble Alpes, F-38042 Grenoble, France

1. Input parameters for MAS-DNP simulations

Below is the list of parameters used in the 3 spins MAS-DNP simulations assuming isotropic relaxation times:

- 3 g-values, $\mathbf{[g_x, g_y, g_z]}$
- 1 electron-electron dipolar coupling, $D_{a,b}$
- 1 electron-electron exchange interaction, $J_{a,b}$
- 1 hyperfine coupling electron-proton, $A_{a,1}$
- 3 hyperfine coupling values for e-^{14}N, $[A_x^{14N}, A_y^{14N}, A_z^{14N}]$
- 3 Euler angles for g-tensor relative orientation, $\Omega_{a,b} = [\alpha, \beta, \gamma]$
- 2 Euler angles for electron-proton dipolar couplings, $[\phi_1, \theta_1]$
- 2 Euler angles for electron-electron dipolar couplings $[\phi, \theta]$
- Electron longitudinal and transverse relaxation times T_{1e} and T_{2e}
- Nuclear longitudinal and transverse relaxation times T_{1n} and T_{2n}
- Microwave nutation frequency, ω_1

Table S1: (left) List of the parameters used to perform the MAS-DNP simulations reported in this work, (right) the method that was used to measure/estimate their values.

Parameter	Evaluation method
$\mathbf{[g_x, g_y, g_z]}$	DFT calculation then HF-EPR fitting
$\boldsymbol{D_{a,b}}$	DFT calculation then HF-EPR fitting
$\boldsymbol{J_{a,b}}$	HF-EPR fitting
$\boldsymbol{A_{a,1}}$	Fitting of the build-up time
$[\boldsymbol{A_x^{14N}, A_y^{14N}, A_z^{14N}}]$	literature then HF-EPR fitting
$\boldsymbol{\Omega_{a,b} = [\alpha, \beta, \gamma]}$	DFT calculation then HF-EPR fitting
$[\boldsymbol{\phi, \theta}]$	DFT calculation then HF-EPR fitting
$[\boldsymbol{\phi_1, \theta_1}]$	Extracted from our spin system
T_{1e} and T_{2e} and orientation dependence	Measured by HF-EPR
T_{1n} and T_{2n}	Fitting of the build-up time for T_{1n}
$\boldsymbol{\omega_1}$	Estimated to best match the experimental and simulated field profiles

2. Hamiltonian

The MAS-DNP simulations use the same Hamiltonian described elsewhere.[1–4] The 3-spin systems are composed of two electrons and one proton {^{1}H-e$_a$-e$_b$}. In the µw rotating frame, the time-dependent Hamiltonian can be written as:

$$\hat{H}(t) = \hat{H}_Z(t) + \hat{H}_{HF}(t) + \hat{H}_D(t) + \hat{H}_J + \hat{H}_{\mu w}$$
$$= \hat{H}_0(t) + \hat{H}_{\mu w}$$

where

$$\hat{H}_Z(t) = \sum_i \left(g_i(t)\beta_e B_0 - \omega_{\mu w}\right)\hat{S}_{z,i} + m_{I,i}A^N_{z,i}(t)\hat{S}_{z,i} - \omega_n \hat{I}_{z,n}$$

$$\hat{H}_{HF}(t) = \sum_i \{A_{z,i,n}(t)\hat{S}_{z,i}\hat{I}_{z,n} + 2(A^+_{i,n}(t)\hat{S}_{z,i}\hat{I}^+_n + A^-_{i,n}(t)\hat{S}_{z,i}\hat{I}^-_n)\}$$

$$\hat{H}_D(t) = D_{a,b}(t)(2\hat{S}_{z,\mathrm{a}}\hat{S}_{z,\mathrm{b}} - 1/2(\hat{S}^+_a\hat{S}^-_b + \hat{S}^-_a\hat{S}^+_b))$$

$$\hat{H}_J = -2J_{a,b}(\hat{S}_{z,a}\hat{S}_{z,b} + 1/2(\hat{S}^+_a\hat{S}^-_b + \hat{S}^-_a\hat{S}^+_b))$$

$$\hat{H}_{\mu w} = \sum_i \omega_{1,s}\hat{S}_{x,i}$$

where g_i is the g-tensor value for electron *i*, $\omega_{\mu w}$ the µw irradiation frequency, $A^N_{z,i}$ the secular part of the hyperfine interaction between electron *i* and ^{14}N that bears the radical, ω_n the nuclear Larmor frequency, $A_{i,n}$ the hyperfine coupling between electron i and nucleus n, $D_{a,b}$ the dipolar coupling between electrons *a* and b, and $J_{a,b}$ the exchange interaction between electrons *a* and *b* (the two radical moieties, respectively). The µw Rabi frequency, $\omega_1/2\pi$, is assumed to be small and is treated as a perturbation. Evolution superoperators are calculated as described in detail in ref. [2]. The nuclear Boltzmann enhancement is then calculated as

$$\varepsilon_{\mathrm{B}}(Nt_r) = {Tr(\rho(Nt_{\mathrm{r}})\hat{I}_z)}\Big/{Tr(\rho(0)\hat{I}_z)}$$

3. Code Extension

The effect of moderate dipolar/J exchange interaction splitting has been accounted for in the μw rotor-events. Using the definitions presented in reference [5], only the microwave off-resonance has been modified. For electron *a* or *b* the frequency offset becomes

$$\Delta\omega_{a/b} = \omega_{a/b} - \omega_{\mu\mathrm{w}} + m_s^{a/b} \times (D_{a,b} - J_{a,b})$$

Where $\omega_{a/b}$ is the Zeeman frequency, $\omega_{\mu w}$ is the microwave frequency and $(D_{a,b} - J_{a,b})$ is the *z* component of the dipolar/exchange interaction. The splitting is reproduced by choosing randomly, for each electron and each crystal orientation, m_s = + ½ or – ½. The approach is valid for dipolar/exchange interactions that are ~1/10 of the EPR linewidth and for temperature/field giving moderate electron polarization (<10 %).

4. Effect of the μw irradiation strength on the DNP field profile

The effect of the microwave irradiation strength/nutation frequency on the DNP field profile of AMUPol, has been calculated and reported in figure S1. As the microwave irradiation strength is changed from 0.1 to 1 MHz, the shape of the DNP field profile is modified. Overall the width defining the positive and negative maxima are broadened for higher microwave irradiation strength. The best match with the experimental data was obtained for a microwave irradiation strength of 0.35 MHz.

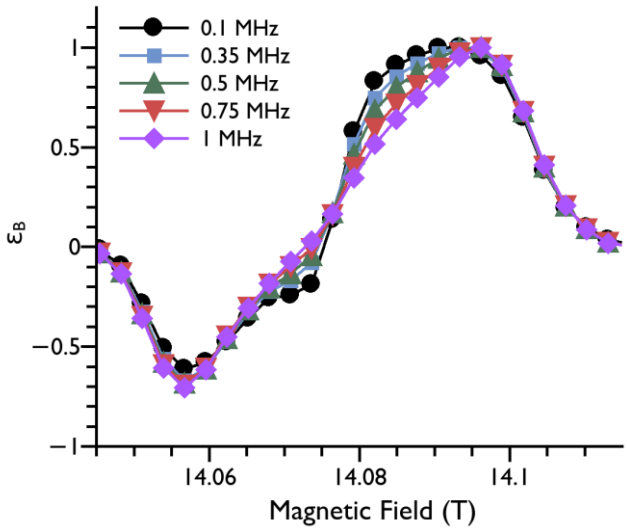

Fig S1. Influence of microwave irradiation strength on the shape of the calculated DNP profile of AMUPol at 14.1 T. black circles corresponds to ω_1= 0.1 MHz, blue squares to 0.35 MHz, up pointing green triangles to 0.5 MHz, down pointing red triangle to 0.75 MHz, purple diamond to 1 MHz.

This value is in line with recent prediction.[6,7]

5. Effect of the magnetic Field on the DNP field profile

Figure S2 (a)/(b) represent the calculated DNP field profile of AMUPol at 9.4 T and TEKPol at 14.1 T respectively.

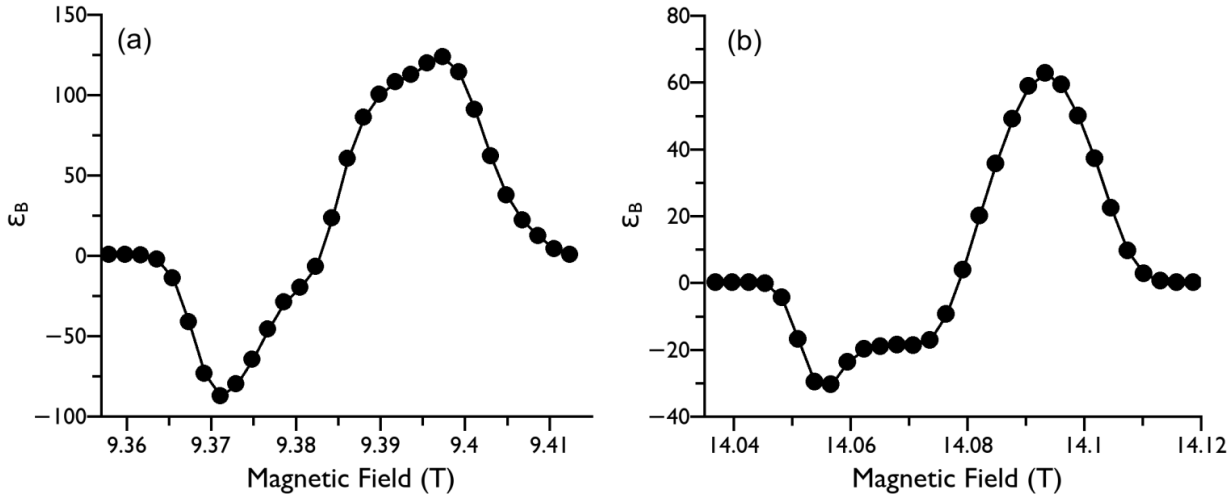

Fig. S2 Calculated MAS-DNP field profile of (a) AMUPol at 9.4 T (b) TEKPol at 14.1 T.

6. Effect of the T_{1e} orientation dependence on the DNP field profile

Figure S3 reports DNP field profiles of AMUPol at 14.1 T with or without considering the orientation dependence of the electron relaxation times. While most of the spectral features of the DNP field profile are maintained, the presence of T_{1e} anisotropy clearly modifies the relative ratio between the positive and negative parts of the DNP field profile. The experiments are better reproduced when accounting for the T_{1e} anisotropy.

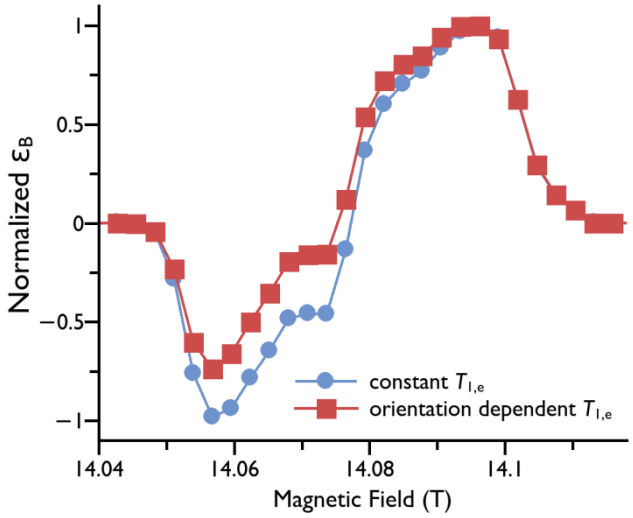

Fig. S3 Calculated MAS-DNP field profile of AMUPol at 14.1T blue circles corresponds to a constant $T_{1,e}$ = 0.4 ms, red squares considers the orientation dependence reported in the main manuscript.

7. Multi-nuclei simulation parameters

The simulations were performed using a fixed magnetic field, μw frequency and MAS frequency. The model is composed of 2 electrons and multiple protons, for which more details can be found in our previous work.[5]. The "local" protons are connected via hyperfine couplings (greater than the MAS frequency) to one of the two electrons, and among them through dipolar couplings, which propagates the polarization from close to distant protons via nuclear dipolar rotor events. The simulations assume the local protons are distributed in a cone along the x-axis of the g tensor. More precisely, these protons are placed within a 4π/9 solid angle cone, in 5 equally spaced layers that provide a proton concentration close to the experimental conditions. The four closest protons have a hyperfine coupling of ~3 MHz. The 5th layer of "local" protons is connected to bulk protons. Each of these bulk nuclei is connected to 6 neighbouring nuclei. For each powder orientation, the local nuclei positions are randomly computed.

Parameters for the simulations are reported in the table S2.

Table S2: parameters used for the multi-nuclei MAS-DNP simulations.

Radical	TEKPol	AMUPol	AMUPol
Magnetic Field (T)	9.403	9.404	14.0925
μw frequency (GHz)	263.73	263.73	395.175
MAS frequency (kHz)	8	8	8
Hyperfine coupling to the closest protons (MHz)	3	3	3
Number of closest protons	4	4	4
Number of layers	5	5	5
Number of local protons	220	220	220
Total number of protons	437	476	476
Cone solid angle	4π/9	4π/9	4π/9

Nuclear T_{2n} (ms)	20	20	20
Mean nuclear dipolar coupling between neighboring protons (kHz)	3.70	2.77	2.77
Equivalent Diffusion Constant[8] (nm^2/ms)	0.00056	0.00038	0.00038
Proton Concentration (M)	13.3	9.6	9.6
$T_{1,n}$ closest protons (s)	0.1	0.1	0.1
$T_{1,n}$ Bulk (s)	5.6	65[3]	76[4,9]

Figure S4 represents an example of the local protons' distribution within the cone in the case of AMUPol. An example of the geometry as an .xyz file can be provided upon request.

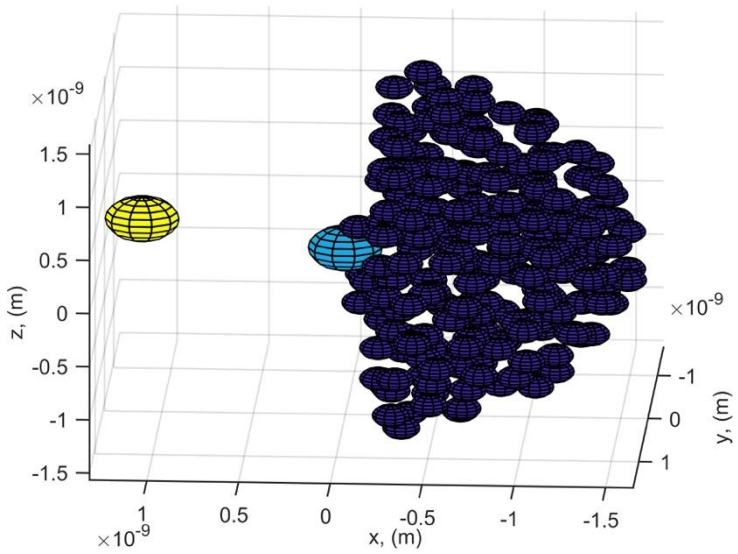

Fig. S4 Example of two electrons and the cone of local protons for AMUPol.

Figure S5 reports the dependence of the polarization gain ϵ_B and the build-up time T_B on the bulk nuclear relaxation $T_{1n,Bulk}$. The computations were performed in the AMUPol (figure S5 (a)) and TEKPol (figure S5 (b)) cases. The observed trends matches previous reports:[5] as the nuclear bulk relaxation increases, both the polarization gain and the build-up times do so until reaching a plateau.

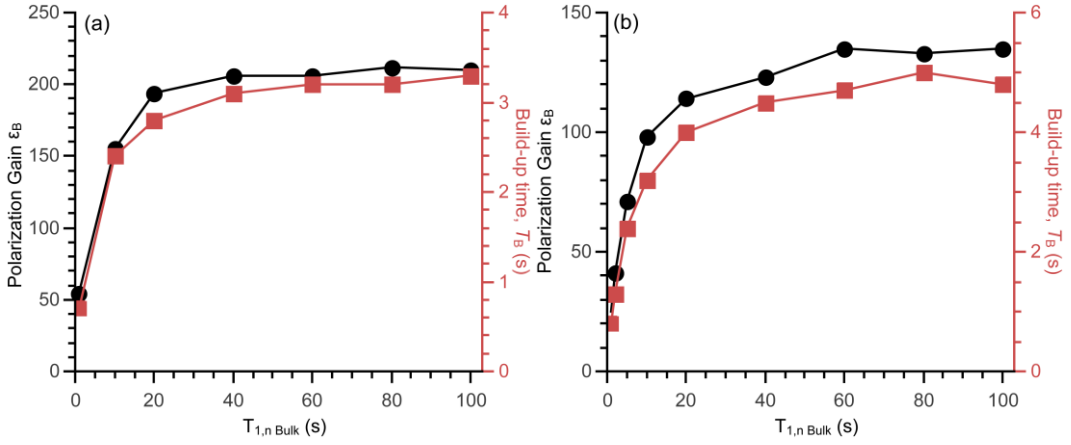

Fig. S5 Effect of $T_{1n,Bulk}$ on the polarization gain ϵ_B (black circles) and the build-up time T_B (red squares) in the case of AMUPol (a), and TEKPol (b). For theses simulations only 377 ZCW orientations have been used.

8. On the prediction capability of the MAS-DNP simulations

Table S3 reports the correcting factors obtained by comparing the Box model assuming interacting or isolated biradicals.

Table S3. $\epsilon_{\mathrm{Depo}}, \epsilon_{\mathrm{on/off}}$ and polarization build-up time T_{B} measured experimentally at 110 K and 10 kHz MAS frequency and simulated using similar input conditions for the box models (isolated and interacting), the multi-nuclei model, and the extrapolated approach. The calculations were performed for 10 mM AMUPol in Glyerol-D_8/D_2O/H_2O (6/3/1 %v) and 15 mM TEKPol in $CHCl_3$/TBE/MeOH-D_4 (65/30/5 %v), where biradical concentration and nuclear spin concentration/relaxation properties are required. For the Glyerol-D_8/D_2O/H_2O (6/3/1 %v) matrix, $T_{1,n}^{\mathrm{Bulk}} = 65$ s at 9.4 T[3] and 76 s at 14.1 T[9], and the ratio ^{1}H/nitroxide = 476. For $CHCl_3$/TBE/MeOH-D_4 (65/30/5 %v), $T_{1,n}^{\mathrm{Bulk}} = 5.6$ s at 9.4 T, and the ratio ^{1}H/nitroxide = 437.

Biradical	Experiment $\epsilon_B/\epsilon_{\mathrm{Depo}}/\epsilon_{\mathrm{on/off}}$	Simulation $\epsilon_B/\epsilon_{\mathrm{Depo}}/\epsilon_{\mathrm{on/off}}$ (Multi-nuclei)	Simulation $\epsilon_B/\epsilon_{\mathrm{Depo}}/\epsilon_{\mathrm{on/off}}$ (isolated box model)	Simulation $\epsilon_B/\epsilon_{\mathrm{Depo}}/\epsilon_{\mathrm{on/off}}$ (interacting box model)	Simulation $\epsilon_B/\epsilon_{\mathrm{Depo}}/\epsilon_{\mathrm{on/off}}$ (Multi-nuclei corrected)	Calculated T_B and build-down time T_{d} (s)
AMUPol at 9.4 T	85/0.40/210	208 / 0.64 / 325	227 / 0.66 / 343	125/0.38/328	114/ 0.38/ 300	3.2/3.6
AMUPol 14.1 T	70/0.55/128	147 / 0.71 / 207	185 / 0.66 / 280	107 / 0.46 / 232	83 / 0.5 / 170	5.2/5.6
TEKPol at 9.4 T	73/0.60/118	108 / 0.81 /1 33	198/0.58/343	108 / 0.39 / 278	60 / 0.54/ 110	2.6/2.7

References

1 F. Mentink-Vigier, U. Akbey, Y. Hovav, S. Vega, H. Oschkinat and A. Feintuch, Fast passage dynamic nuclear polarization on rotating solids, *J. Magn. Reson.*, 2012, **224**, 13–21.

2 F. Mentink-Vigier, U. Akbey, H. Oschkinat, S. Vega and A. Feintuch, Theoretical aspects of Magic Angle Spinning - Dynamic Nuclear Polarization, *J. Magn. Reson.*, 2015, **258**, 102–120.

3 F. Mentink-Vigier, S. Paul, D. Lee, A. Feintuch, S. Hediger, S. Vega and G. De Paëpe, Nuclear depolarization and absolute sensitivity in magic-angle spinning cross effect dynamic nuclear polarization, *Phys. Chem. Chem. Phys.*, 2015, **17**, 21824–21836.

4 F. Mentink-Vigier, G. Mathies, Y. Liu, A.-L. Barra, M. A. Caporini, D. Lee, S. Hediger, R. G. Griffin and G. De Paëpe, Efficient cross-effect dynamic nuclear polarization without depolarization in high-resolution MAS NMR, *Chem. Sci.*, 2017, **8**, 8150–8163.

5 F. Mentink-Vigier, S. Vega and G. De Paëpe, Fast and accurate MAS–DNP simulations of large spin ensembles, *Phys. Chem. Chem. Phys.*, 2017, **19**, 3506–3522.

6 B. J. Albert, S. Ho Pahng, N. Alaniva, E. L. Sesti, P. W. Rand, E. P. Saliba, F. J. Scott, E. J. Choi and A. B. Barnes, Instrumentation for Cryogenic Magic Angle Spinning Dynamic Nuclear Polarization using 90 Liters of Liquid Nitrogen Per Day, *J. Magn. Reson.*, , DOI:10.1016/j.jmr.2017.08.014.

7 D. J. Kubicki, A. J. Rossini, A. Purea, A. Zagdoun, O. Ouari, P. Tordo, F. Engelke, A. Lesage and L. Emsley, Amplifying Dynamic Nuclear Polarization of Frozen Solutions by Incorporating Dielectric Particles, *J. Am. Chem. Soc.*, 2014, **136**, 15711–15718.

8 A. Karabanov, D. Wiśniewski, I. Lesanovsky and W. Köckenberger, Dynamic Nuclear Polarization as Kinetically Constrained Diffusion, *Phys. Rev. Lett.*, 2015, **115**, 020404.

9 G. Mathies, M. A. Caporini, V. K. Michaelis, Y. Liu, K.-N. Hu, D. Mance, J. L. Zweier, M. Rosay, M. Baldus and R. G. Griffin, Efficient Dynamic Nuclear Polarization at 800 MHz/527 GHz with Trityl-Nitroxide Biradicals, *Angew. Chem. Int. Ed.*, 2015, **127**, 11936–11940.